Feasibility Study of Controlled-Source Electromagnetic Method for Monitoring Low-Enthalpy Geothermal Reservoirs

Eltayieb, Mahmoud; Werthmüller, Dieter; Drijkoningen, Guy; Slob, Evert

DOI
10.3390/app13169399

Publication date
2023

Document Version
Final published version

Published in
Applied Sciences

Citation (APA)
Eltayieb, M., Werthmüller, D., Drijkoningen, G., & Slob, E. (2023). Feasibility Study of Controlled-Source Electromagnetic Method for Monitoring Low-Enthalpy Geothermal Reservoirs. *Applied Sciences*, *13*(16), Article 9399. https://doi.org/10.3390/app13169399

applied sciences

MDPI

Article

Feasibility Study of Controlled-Source Electromagnetic Method for Monitoring Low-Enthalpy Geothermal Reservoirs

Mahmoud Eltayieb [1,2,*], Dieter Werthmüller [1], Guy Drijkoningen [1] and Evert Slob [1]

[1] Department of Geoscience and Engineering, Delft University of Technology, Stevinweg 1, 2628 CN Delft, The Netherlands; d.werthmuller@tudelft.nl (D.W.); g.g.drijkoningen@tudelft.nl (G.D.); e.c.slob@tudelft.nl (E.S.)

[2] Department of Earth Sciences, Swiss Federal Institute of Technology in Zürich, Sonneggstrasse 5, 8006 Zürich, Switzerland

* Correspondence: m.f.m.i.eltayieb@tudelft.nl

Abstract: Tracking temperature changes by measuring the resulting resistivity changes inside low-enthalpy reservoirs is crucial to avoid early thermal breakthroughs and maintain sustainable energy production. The controlled-source electromagnetic method (CSEM) allows for the estimation of sub-surface resistivity. However, it has not yet been proven that the CSEM can monitor the subtle resistivity changes typical of low-enthalpy reservoirs. In this paper, we present a feasibility study considering the CSEM monitoring of 4–8 Ω·m resistivity changes in a deep low-enthalpy reservoir model, as part of the Delft University of Technology (TU Delft) campus geothermal project. We consider the use of a surface-to-borehole CSEM for the detection of resistivity changes in a simplified model of the TU Delft campus reservoir. We investigate the sensitivity of CSEM data to disk-shaped resistivity changes with a radius of 300, 600, 900, or 1200 m at return temperatures equal to 25, 30, . . . , 50 °C. We test the robustness of CSEM monitoring against various undesired effects, such as random noise, survey repeatability errors, and steel-cased wells. The modelled differences in the electric field suggest that they are sufficient for the successful CSEM detection of resistivity changes in the low-enthalpy reservoir. The difference in monitoring data increases when increasing the resistivity change radius from 300 to 1200 m or from 4 to 8 Ω·m. Furthermore, all considered changes lead to differences that would be detectable in CSEM data impacted by undesired effects. The obtained results indicate that the CSEM could be a promising geophysical tool for the monitoring of small resistivity changes in low-enthalpy reservoirs, which would be beneficial for geothermal energy production.

Keywords: low-enthalpy reservoirs; TU Delft campus geothermal project; geothermal energy; sustainable utilization; CSEM monitoring; feasibility study

Citation: Eltayieb, M.; Werthmüller, D.; Drijkoningen, G.; Slob, E. Feasibility Study of Controlled-Source Electromagnetic Method for Monitoring Low-Enthalpy Geothermal Reservoirs. *Appl. Sci.* **2023**, *13*, 9399. https://doi.org/10.3390/app13169399

Academic Editor: Giuseppe Lacidogna

Received: 5 July 2023
Revised: 11 August 2023
Accepted: 16 August 2023
Published: 18 August 2023

1. Introduction

District heating consumes about half of the energy produced worldwide [1,2]. Most of this energy is generated by burning fossil fuels, which contributes to global warming [3,4]. Low-enthalpy reservoirs provide geothermal energy for heating and cooling, both in residential and industrial applications [5]. Low-enthalpy energy is renewable energy, which makes it important in the pursuit to mitigate global warming. Low-enthalpy reservoirs are sub-surface layers of water-filled rocks at temperatures below 150 °C [6–8]. Energy can be produced from these reservoirs by pumping out hot water, extracting the heat, and then re-injecting it at lower temperatures [9,10]. The re-injected water spreads around the return well and forms a cold plume [11], which maintains the volume of the geothermal reservoir but leads to a long-term temperature decline [12]. The cold plume grows depending on the production rate and, if not managed properly, can result in an early thermal breakthrough, where the cold plume reaches the producing well. As a result, energy production may decrease to a level that it is no longer profitable [13].

Efficient management of production helps to avoid early thermal breakthroughs, which can be achieved by determining a level of sustainable utilization that can be maintained for many decades [14–16]. For this purpose, reservoir simulation is typically used to predict the development of the cold plume in many production scenarios [17]. However, uncertainty in the petrophysical characteristics of the reservoir, such as its porosity and permeability, can lead to predictions that differ from actual future production [18]. Therefore, it is necessary to monitor the cold plume in real-time to calibrate reservoir simulations and predict energy production more accurately. In this paper, we focus on monitoring the cold plume in the low-enthalpy reservoir of the TU Delft campus geothermal project, which is a well doublet that is under construction [19].

Geophysical methods, such as seismic and electromagnetic (EM), provide valuable information regarding the physical properties of reservoirs for characterization and monitoring. Seismic methods utilise the elastic structure of the earth [20], while EM methods explore the electrical resistivity [21,22]. At a fixed salinity, the electrical resistivity of a fluid filling rock pores is inversely proportional to its temperature [11,23]. Therefore, the electrical resistivity of the TU Delft campus reservoir can be expected to increase at a percentage as the temperature decreases. EM techniques, such as electrical resistivity tomography (ERT), magnetotellurics (MT), and the CSEM, are suitable for mapping resistivity changes as an indicator of the cold plume.

The length of the ERT acquisition profile is normally several times the investigated depth [24]. To monitor the deep TU Delft campus reservoir, ERT surveys require an acquisition profile many kilometres deep, which is not feasible. MT can achieve a great depth of investigation by measuring the sub-surface response to naturally occurring EM fields [25]; however, MT measurements suffer from a low signal-to-noise ratio (SNR) in urban environments [26,27], and may not be able to detect small resistivity changes due to variations in MT fields [28]. The CSEM relies on artificial sources of EM fields to investigate the electrical resistivity of the sub-surface to a depth of a few kilometres [29,30]. CSEM fields suffer from less variation due to the high repeatability of the source fields, and are characterised by high SNR due to the high source power [31]. Overall, we purpose CSEM to monitor the resistivity changes in the TU Delft campus geothermal reservoir.

Several configurations can be used to collect CSEM monitoring data, such as surface-to-surface, surface-to-borehole, borehole-to-surface, and/or borehole-to-borehole. The surface-to-surface configuration allows for dense data coverage at relatively low cost. The TU Delft campus reservoir lies at such a depth that CSEM fields carrying information about the resistivity change will be below the noise floor when collecting surface-based measurements. Furthermore, deploying the receivers at the surface makes them susceptible to high levels of both natural and anthropogenic noise. In surface-to-borehole and borehole-to-surface configurations, electric fields travel relatively short distances and can be measured with amplitudes above the noise floor. While the surface-to-borehole configuration is theoretically equivalent to the borehole-to-surface, practical applications indicate that the surface-to-borehole configuration offers a relatively higher SNR for two reasons: (1) The ability to achieve large dipole moments with surface sources, and (2) the borehole receivers are located away from EM noise near the surface [32,33]. The borehole-to-borehole CSEM requires a borehole source, has a limited dipole moment, and only provides two-dimensional (2D) inter-well resistivity information.

In this paper, we investigate the feasibility of CSEM monitoring for 4–8 Ω·m resistivity changes in the deep low-enthalpy reservoir model of the TU Delft campus geothermal project. Considering the reasons mentioned above, we chose to use a surface-to-borehole configuration to determine time-lapse electric fields (i.e., fields with temporal intervals). Monitoring this low-enthalpy reservoir is a process that will be carried out over several decades, as the resistivity change is expected to progress laterally. We explore the potential of the CSEM technique to monitor various lateral resistivity changes inside the TU Delft campus low-enthalpy reservoir. We also test the robustness of the CSEM monitoring of the reservoir against undesired effects, which can distort CSEM data when scattered by the

reservoir. These effects include multiplicative random noise, survey repeatability errors, near-surface changes, and the influence of a steel-cased borehole. To date, there has been no investigation on the impact of the high magnetic permeability and the low electrical resistivity of a steel casing on surface-to-borehole CSEM data. Thus, we incorporated the magnetic and electric properties of the steel casing into the model, in order to study its effect on the vertical electric field. Due to the advantages that composite pipes have over steel ones during geothermal operations, composite pipes will replace steel pipes in the near future [34]. To evaluate the effect of the composite casing on the CSEM response, we changed the properties of the casing from those of steel to fibreglass-reinforced epoxy. In general, this paper details a forward modelling framework suggesting the feasibility of the CSEM monitoring of low-enthalpy reservoirs with distorted time-lapse data.

The remainder of this paper is structured as follows. In Section 2, we give a brief description of the geological and electrical resistivity models of the TU Delft campus sub-surface. In Section 3, we briefly mention the two CSEM forward-modelling approaches used in this study. In Section 4, we explore useful source locations for the CSEM monitoring of the TU Delft campus reservoir with preferential acquisition parameters; namely, the source–receiver setup and the source frequency. In Section 5, we assess the feasibility of using a time-lapse CSEM to track the time-lapse resistivity changes resulting from different return temperatures. In Section 6, we assess the robustness of CSEM monitoring when undesired effects corrupt the time-lapse signal. In Section 7, we discuss the merits and limitations of this feasibility study. In Section 8, we draw conclusions regarding the feasibility of CSEM monitoring the TU Delft campus low-enthalpy reservoir.

2. TU Delft Campus Geothermal Project

The low-enthalpy reservoir of the TU Delft campus geothermal project lies in the West Netherlands Basin, an inverted rift basin. The stratigraphical setting of the West Netherlands Basin down to 3 km depth and the resistivity of the layers (obtained from logs) are shown in Figure 1 [35]. The target low-enthalpy reservoir is the Delft Sandstone Member, located at a depth of 2.3 km. The porosity and permeability of the Delft Sandstone member reach 30% and 1130 mD, respectively [36]. Temperature logs from exploration wells in the region indicate a gradient of 30 °C/km. Therefore, the water temperature of the Delft Sandstone Member is expected to be around 75 °C. Overall, the Delft Sandstone Member has aquifer qualities suitable for geothermal energy production.

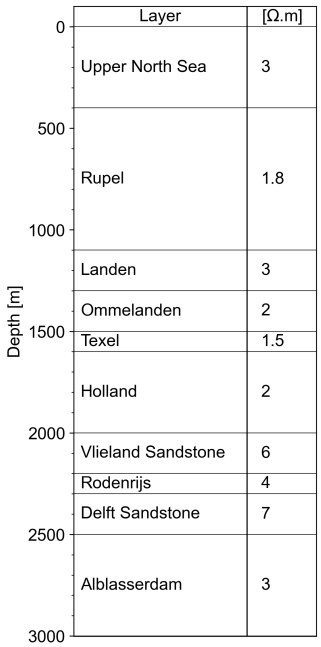

Figure 1. Sub-surface layers under the TU Delft campus and their average depth and resistivity.

A geothermal doublet is planned to be installed on the campus of TU Delft, in order to supply heating to the campus buildings. The doublet design, as shown in Figure 2, involves a production well and an injection well that will be drilled vertically next to each other in the first 0.8 km. Then, the boreholes deviate from vertical with different dips and azimuths, until they reach the reservoir with 1.5 km separation. After heating the campus buildings, the discharge water will be injected into the reservoir at a temperature between 30–50 °C, depending on the heat demand [37].

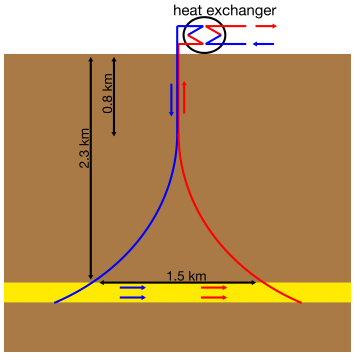

Figure 2. Doublet well design for TU Delft campus geothermal project. The well separation at the surface is 10 m. The red and blue arrows refer to the direction of hot and cold water, respectively.

The change in electrical resistivity of a pore-filling fluid with temperature can be determined from the following equation [38]:

$$R_{(T_2)} = R_{(T_1)}[1 + \alpha(T_2 - T_1)], \tag{1}$$

where $R_{(T_1)}$ and $R_{(T_2)}$ are the electrical resistivities at a base temperature, T_1, and a monitoring temperature, T_2, respectively; and α refers to the temperature coefficient of resistivity, which has a value of 0.025 $^{\circ}C^{-1}$ for most brines [38]. According to Equation (1), the electrical resistivity of the TU Delft campus reservoir will change from 7 Ω·m to 11 Ω·m with a temperature drop from 75 °C to 50 °C.

3. Methods

We use two frequency-domain EM (FDEM) forward-modelling approaches to study the feasibility of CSEM monitoring the TU Delft campus reservoir: (1) A one-dimensional (1D) reflectivity formulation for a layered model [39], in order to find a preferential survey configuration and source frequency at a low computational cost. This approach is implemented by [40]; (2) a finite-integration technique to determine the electric field response in a three-dimensional (3D) medium, as coded by [41]. We use the latter approach to investigate the source–receiver offsets, the sensitivity of CSEM data to volumetric and incremental changes, and the impacts of undesired effects.

To assess the CSEM detectability of the resistivity changes, we define confidence intervals for the difference between time-lapse electric fields. We treat differences below 1% as undetectable, while differences between 1% and 10% offer low confidence, those between 10% and 30% moderate confidence, and differences greater than 30% high confidence. We define these intervals based on the influence of the undesired effects in Section 6. The difference ΔE between the electric field of the base state E_1 and the monitoring state E_2 is given by

$$\Delta E = \frac{\|E_2 - E_1\|}{\|E_1\|}, \tag{2}$$

where $\|\ldots\|$ refers to the absolute value. We mask the time-lapse electric fields and difference when the amplitude of E_1 or E_2 is below the noise floor. The noise floor of electric field data is frequency-dependent [42]. In [43], it was shown that the noise floor decreases with increasing frequency until it reaches about 4×10^{-12} V/m for frequencies equal to or greater than 1 Hz. For simplicity, we set a noise floor of 10^{-12} V/m for all frequencies.

4. Source–Injection–Borehole Offset

We consider the CSEM monitoring of the TU Delft campus reservoir with source offsets 1, 2, and 3 km from the injection well, which has zero offset. The source is an x-directed electric dipole. We carried out 1D numerical experiments to evaluate the source frequency and sensitivity of the EM components to the resistivity change. The results indicate that the vertical electric field is the most sensitive to the changes, and that a source frequency around 1 Hz offers an adequate depth of propagation and resolving power. The resistivity change has a disk shape with 300 m radius, centred at the injection well. The radius of the change is one-fifth the distance between the injector and the producer. The survey domain was discretized with a uniform grid spacing of 50 m along the polar and longitudinal axes, while the azimuthal direction was divided into 40 segments of 9°.

Figure 3 shows the z-component of the electric field for different source offsets. Changing the source offset from 1 to 3 km did not change the magnitude of the difference; however, it affected the amplitude of the electric fields reaching the resistivity change and, subsequently, the ability to monitor the 300 m resistivity change. At an offset of 1 or 2 km, the monitoring electric fields can cover the resistivity change and the area around it. A difference of moderate confidence was observed within and around the location of the resistivity change. As the time-lapse fields were scattered around the resistivity change, a difference of low confidence could be determined some distance away. A source offset of 3 km led to a difference of the back-scattered field in a relatively small area. This limits the freedom of measurement for the difference of the forward-scattered field, especially in the case of cold fronts with larger radii. Consequently, we set a source offset in the range of 1–2 km with 1 Hz frequency to acquire vertical electric fields for the monitoring of resistivity changes in the TU Delft campus reservoir model.

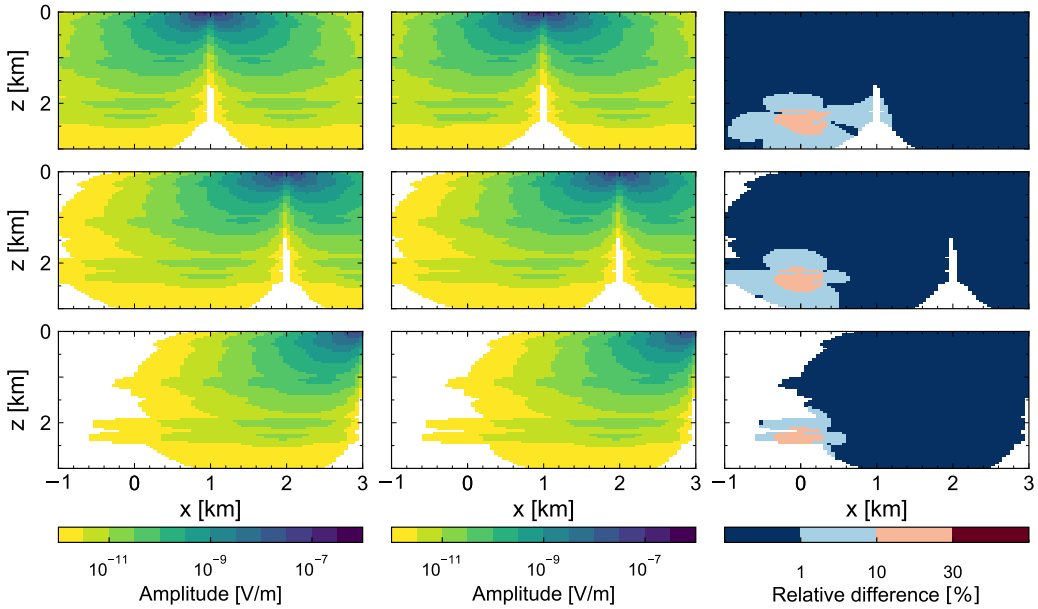

Figure 3. Time-lapse electric field response and difference at different source offsets (1, 2, or 3 km from (**top**) to (**bottom**)). The (**left column**) shows the electric field response of the base model, the (**middle column**) shows that of the monitoring model, and the (**right column**) provides their relative difference.

5. Temperature Effects

The CSEM method was able to detect the subtle resistivity changes in the TU Delft campus reservoir with the preferential acquisition setup, as shown in Figure 3. Thus, the CSEM monitoring of the TU Delft campus reservoir allows for tracking the growth of the resistivity change over decades. Hence, we checked whether the time-lapse electric field responses acquired with the surface-to-borehole setup were sensitive to an increased

resistivity change radius. With an expected fluctuation in temperature of the injected water depending on heat demand, the quantity of the resistivity change will fluctuate as well; see Equation (1). Thus, we considered the monitoring of temperature effects under different volumes.

Figure 4 shows the difference in monitoring fields determined at a zero offset for different disk radii and magnitudes of the resistivity change. The source had a frequency of 1 Hz and was located with a 1 km offset. At a certain return temperature, the difference in time-lapse fields increases when increasing the radius of the resistivity change; meanwhile, for a certain radius, the difference increases with temperature. Figure 4 indicates that the time-lapse electric fields acquired with the surface-to-borehole configuration are sensitive to the growth and magnitude of the resistivity change. Considering these results, we next tested the robustness of CSEM monitoring in the presence of undesired effects.

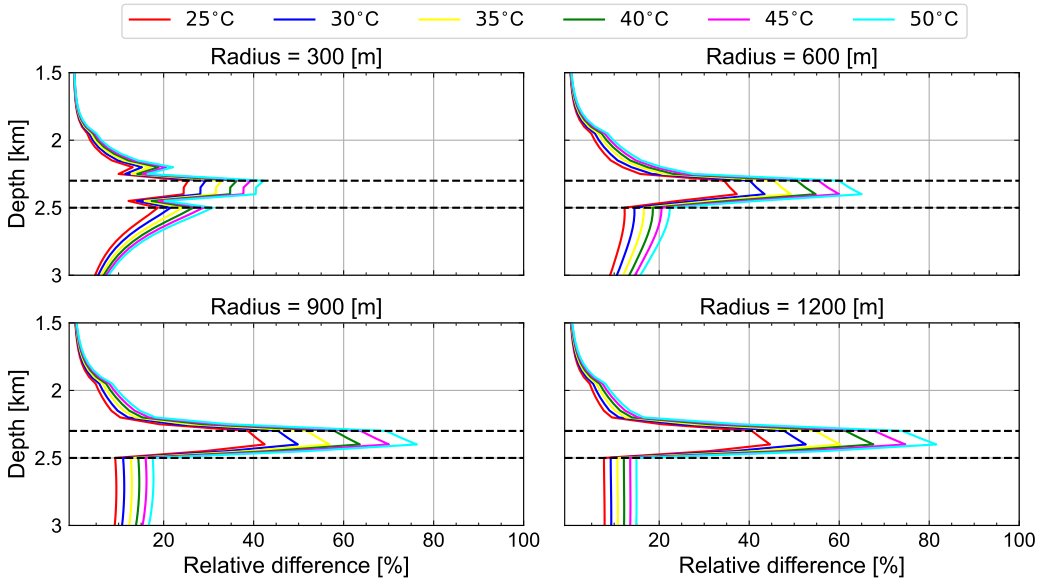

Figure 4. Sensitivity of time-lapse electric fields to volumetric and resistivity changes due to various temperature contrasts. The black dashed lines show the boundaries of the low-enthalpy reservoir at 2.3 and 2.5 km.

6. Undesired Effects

Beside the change in resistivity, there are various effects that also create a difference in the time-lapse fields. As such, these effects may hinder the CSEM monitoring of the resistivity change inside the low-enthalpy reservoir. In this section, we study the impact of undesired effects on the CSEM monitoring of the 300 m radius resistivity change at a 25 °C temperature contrast, which gives the lowest difference. If a time-lapse CSEM can monitor this change in the presence of signal contamination, it will be able to monitor other scenarios of resistivity change, as detailed in Section 5. We consider the following commonly occurring undesired effects.

6.1. Recording Noise

Recording noise involves receiver self-noise, natural, and anthropogenic noise. Receiver self-noise is random noise caused by the sensor thermal noise and the amplifier voltage noise. Receiver self-noise increases with decreasing source frequency, until it steadies at frequencies above 10^{-1} Hz [42]. Anthropogenic noise is periodic and/or random [44]. Periodic noise is generated by power lines, buried metallic cables, grounded electric devices, and so on. Most periodic noise can be heavily attenuated by applying digital filters to data. Random anthropogenic noise, on the other hand, can be caused by sources such as the motion of trains or trams on the rail tracks. Random noise can be diminished by stacking

repeated measurements to increase the signal-to-noise ratio. Increasing the source dipole moment also helps to increase the signal-to-noise ratio.

To account for the recording noise that may not be removed via processing, we changed the amplitude of the electric field randomly in the range of ±1%, as follows:

$$\eta = 0.01[n_1 \Re(E) + \mathrm{i} n_2 \Im(E)], \tag{3}$$

where n_1 and n_2 are random values between $-\sqrt{0.5}$ and $\sqrt{0.5}$; the two symbols $\Re(E)$ and $\Im(E)$ refer to the real and the imaginary parts of the calculated electric field response, respectively; and i refers to the imaginary unit. Different random multiplicative noise was added to the base and monitoring electric fields. The electric fields were determined using the setup detailed in Section 4.

As shown in Figure 5, the resistivity change presented a time-lapse difference that was generally stronger than that of the synthesized recording noise. Random noise in the base and monitoring electric fields can either add or subtract, leading to the amplification or cancellation of the noise in the difference. It is better to reduce the random noise in the data, in order to avoid any possible amplification when calculating the time-lapse difference. After describing the irregular errors arising from random noise, we analyse the errors arising from unrepeatable survey factors.

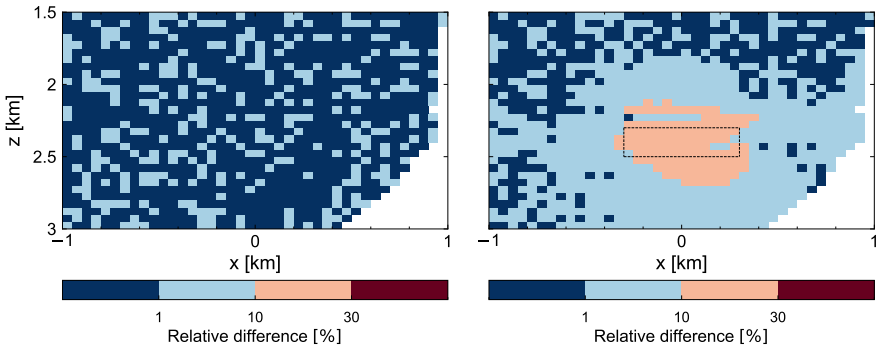

Figure 5. The influence of 1% recording noise when monitoring the 300 m radius change. The (**left plot**) shows the relative difference due to the random noise, while the (**right plot**) shows the relative difference between the base and monitoring fields in the presence of the recording noise. The black dashed rectangle indicates the boundaries of the resistivity change.

6.2. Survey Repeatability Errors

Repeatability errors are generated by inexact positioning and/or orientation of the receivers and the source in time-lapse surveys. In a surface-to-borehole survey, wireline receivers are installed in a vertical monitoring well. Replacing aged borehole receivers may change the location of the receivers while their orientation remains fixed. Regarding the surface source, the location, azimuth, and frequency may change. The authors of [45] added 1% error relative to the signal amplitude to mimic repeatability errors in surface-to-surface surveys. Here, we adopt a different approach to study the impact of 1% repeatability errors on a surface-to-borehole CSEM. We changed the source location, azimuth, and frequency by 10 m, 1°, and 0.01 Hz, respectively, and arbitrarily changed the position of the receivers by 5 m.

Figure 6 shows that the difference resulting from the survey errors was typically in the range of 1–10%, and even exceeded 10% in the 200 m around the zero-crossing. This high error near the zero-crossing was caused by the source repeatability error, as the error decreased when moving away from the source. As the source was 700 m from the edge of the resistivity change, it would still be possible to detect a difference with moderate confidence due to the resistivity change. This implies that the impact of the source repeatability error is reduced when the source is at an adequate distance from the borehole receivers. Next, we examined data errors caused by seasonal near-surface changes.

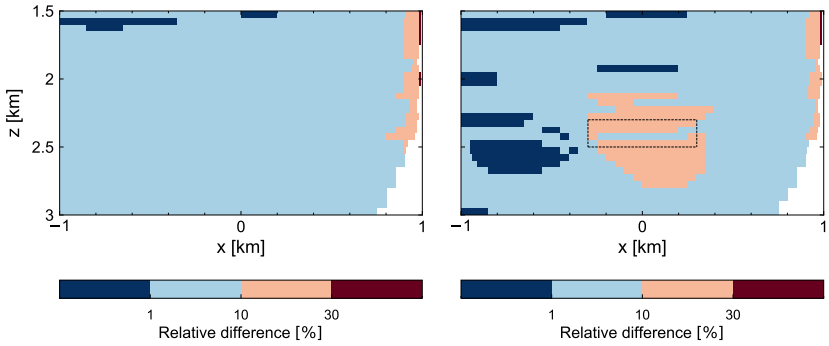

Figure 6. Time-lapse monitoring of the TU Delft campus reservoir with errors in the source and receiver parameters. The (**left plot**) shows the relative difference due to the repeatability error, while the (**right plot**) shows the difference due to the repeatability error and resistivity change.

6.3. Near-Surface Temperature Change

Near-surface changes are commonly caused by seasonal variations in the temperature of the soil, which is in contact with the atmosphere. In particular, seasonal variation in the near-surface temperature alters the time-lapse electric field. In the Netherlands, the average minimum and maximum temperatures at 1 m depth are 8 °C and 17 °C, respectively, while the temperature gradient in the soil is about 4.2 °C/m [46]. The temperature gradient takes a negative value in the summer and a positive value in the winter. At a depth of 2 m, the soil temperature remains almost the same through all seasons. To include the effect of seasonal near-surface variation, we increased the electrical resistivity in the first two meters of the upper layer by 112.5% (see Equation (1)).

The effect of the near-surface resistivity change, as shown in Figure 7, did not reach the reservoir. The CSEM fields are sensitive to the conductivity–thickness product of the layers, and the near-surface change occurs over only a slight thickness. Therefore, it did not produce a large difference in time-lapse fields. More importantly, the near-surface change has a limited area of influence in the shallow sub-surface and, so, does not interfere with the monitoring of the low-enthalpy reservoir at depth. After examining the errors from near-surface changes, we investigated the impact of a steel casing on the electric field.

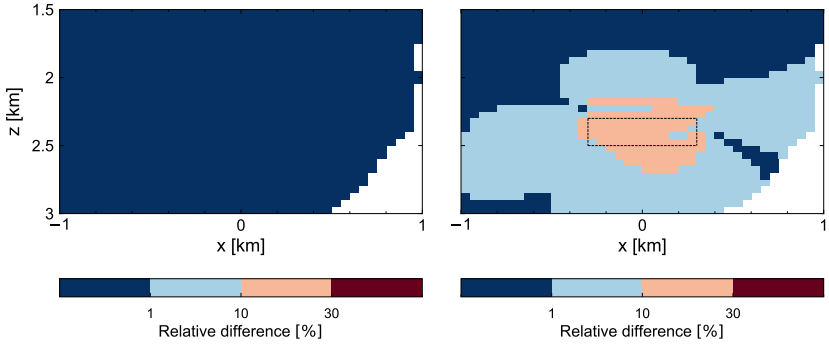

Figure 7. Time-lapse monitoring of the TU Delft campus reservoir in the presence of sub-surface changes. The (**left plot**) shows the relative difference due to the 9 °C seasonal variation in soil temperature, while the (**right plot**) shows the difference due to the seasonal variation and resistivity changes.

6.4. Casing Effect

As mentioned in Section 2, the design of the TU Delft geothermal doublet includes two deviated steel-cased wells. The impact of the very low electrical resistivity of the steel casing on the EM field response is significant [47–50]. In [51], it was shown that it is also important to take into account the high magnetic permeability of the steel casing when conducting CSEM forward modelling.

Thus, we incorporated the physical properties of a steel-cased vertical well into the TU Delft campus sub-surface model. The thickness of the casing wall is 2.5 cm and its

diameter is 15 cm. The considered steel has an electrical resistivity and a relative magnetic permeability equal to 10^{-6} Ω·m and 100, respectively. The hollow of the casing was assumed to be filled with a brine of resistivity equal to 5.68×10^{-2} Ω·m. The physical properties of the casing do not change over time, corresponding to a non-corroded casing. The model was discretized on a cylindrical mesh. Thus, only the impact of one vertical-cased well could be modelled.

As shown in Figure 8, the modelled steel-cased well severely disturbed the electric field. The steel casing changed the field response by 30% or more within 10 m of its vicinity. The footprint of the steel casing reduced with distance, ranging between 10 and 30% within 100 m and less than 10% further away. Close to the source location, the footprint of the casing was less than 1%, except around the zero-crossing. This significant distortion in the electric field was caused by electric fields induced in the modelled steel medium. These fields propagate into the surrounding environment to distort the electric fields from the source. Figure 8 also shows that the detectability of the resistivity change decreased within 10 m around the steel casing, as well as some other areas within 100 m around the casing. Away from the casing, the resistivity change still created a sufficient difference.

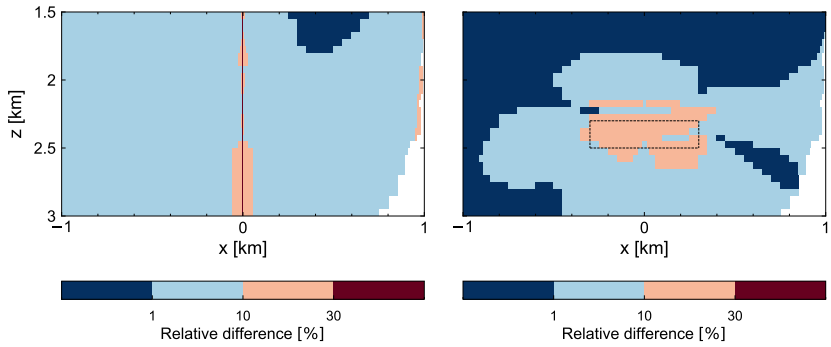

Figure 8. Time-lapse CSEM monitoring of the TU Delft campus reservoir in the presence of a steel casing. The (**left plot**) shows the effect of the steel casing on the electric field response, while the (**right plot**) shows the effect of the steel casing on the difference between time-lapse electric fields.

We changed the properties of the casing from steel to fibreglass-reinforced epoxy, which has resistivity of around 10^{16} Ω·m and unit magnetic permeability. The effect of the composite casing on the electric field was limited to the borehole, and is not observable in Figure 9. Based on the right-hand plots in Figures 8 and 9, it seems that the composite casing had no influence on the electric field outside the casing, allowing for the CSEM monitoring of the geothermal reservoir close to the borehole. The negligible impact of the composite medium can be attributed to its very high electrical resistivity and no magnetization, therefore not producing induction fields.

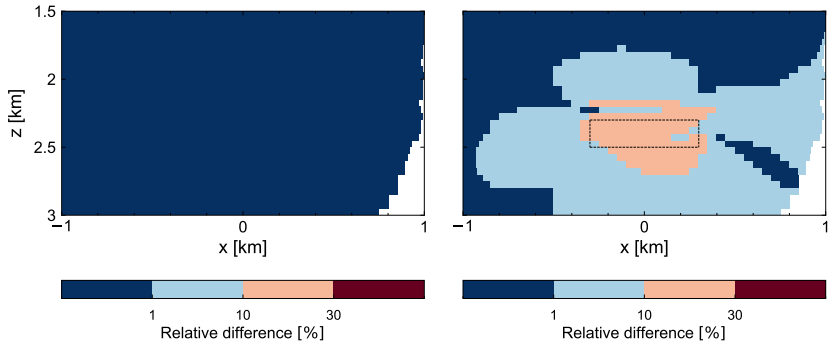

Figure 9. Time-lapse CSEM monitoring of the TU Delft campus reservoir in the presence of a composite casing. The (**left plot**) shows the effect of the composite casing on the electric field response, while the (**right plot**) shows the effect of the composite casing on the difference between time-lapse electric fields.

7. Discussion

We studied the feasibility of CSEM monitoring of resistivity changes in the TU Delft campus reservoir, which involves a custom surface-to-borehole setup. This setup requires the drilling of a monitoring well for the installation of borehole receivers. The forward modelling results did not identify an optimal location for such a monitoring well. An optimized experimental design may help to find such a location. When assessing the location of a monitoring well, the relatively high fluid flow between wells resulting from energy production should be considered. This high fluid flow would cause a sharp edge in the changes toward the production well, which should ideally be monitored.

The results of our study show—as can be observed in Figure 4—that the CSEM method is sensitive to resistivity changes inside the TU Delft geothermal reservoir model, regardless of their radius or magnitude. However, we found that changes of large radius and small magnitude provide the same difference as changes of a small radius and large magnitude, which introduces uncertainty into the interpretation of time-lapse CSEM data. As such, it may be necessary to combine CSEM data with other geophysical data; in particular, coupling it with sub-surface fluid flow models and local temperature and pressure measurements in the injection and monitoring wells is necessary to obtain better insights regarding the changes.

Undesired effects pose significant challenges for CSEM monitoring. These effects distort the field response and can make it difficult to detect resistivity changes. While random recording noise and near-surface changes have a minor impact, survey repeatability errors lead to more severe effects. Close to the source, repeatability errors may generate a difference greater than the difference due to the resistivity change. The steel casing also has a severe impact, heavily damping the vertical electric field in its vicinity. To reduce the sensitivity of CSEM data to severe undesired effects, the data should be collected at least 200 m away from the source and 100 m from steel-cased boreholes. Our results suggest that the CSEM method can provide valuable information about the resistivity changes inside the TU Delft campus reservoir, despite the presence of undesired effects.

8. Conclusions

We demonstrated the feasibility of using the CSEM method to monitor the subtle resistivity changes inside the TU Delft campus low-enthalpy reservoir model. In this feasibility study, we determined a survey design—including the survey configuration, source frequency, and source offset—that allows for the CSEM monitoring of the resistivity changes in the TU Delft campus reservoir with sufficient confidence. The results of the study indicated that the z-component determined with a surface-to-borehole CSEM is sensitive to resistivity changes of different volumes and contrasts, suggesting its suitability for monitoring changes in the reservoir due to heat production over decades.

Through this study, we showed that the CSEM monitoring of the TU Delft campus geothermal reservoir seems possible, even in the presence of undesired effects. Among these effects, survey repeatability errors had the largest impact on CSEM monitoring. The effect of the steel casing was negligible 100 m away from it. When we changed the properties of the casing from steel to composite, we found that the electric field response was only affected within the casing. Generally speaking, the CSEM method with a customized acquisition setup can be used to detect small resistivity changes in the TU Delft campus low-enthalpy reservoir with high confidence, which will not be obscured by undesired effects.

Overall, the results of this feasibility study demonstrate that the CSEM has high potential as a viable technology for monitoring and managing low-enthalpy geothermal reservoirs, such as the TU Delft campus reservoir. The results of our study indicate that time-lapse CSEM surveys can provide information to make well-informed management decisions, possibly extending the production lifetime of low-enthalpy reservoirs. The approach followed in this study can serve as a framework for future CSEM field tests and, when successful, eventually for monitoring campaigns. This also includes monitoring high-enthalpy geothermal reservoirs.

Author Contributions: Conceptualization, M.E., D.W., G.D. and E.S.; methodology, M.E., D.W. and E.S.; software, M.E. and D.W.; validation, M.E., D.W., G.D. and E.S.; formal analysis, M.E., D.W., G.D. and E.S.; investigation, M.E.; resources, G.D.; data curation, M.E.; writing—original draft preparation, M.E.; writing—review and editing, M.E., D.W., G.D. and E.S.; visualization, M.E.; supervision, D.W., G.D. and E.S.; project administration, G.D.; funding acquisition, G.D. All authors have read and agreed to the published version of the manuscript.

Funding: This project received funding from the European Union's Horizon 2020 research and innovation programme under the Marie Skłodowska-Curie grant agreement No. 956965, https://cordis.europa.eu/project/id/956965, accessed on 15 December 2020.

Institutional Review Board Statement: Not applicable.

Informed Consent Statement: Not applicable.

Data Availability Statement: All data and Python scripts supporting the findings of this study are available upon request from the corresponding author.

Conflicts of Interest: The authors declare no conflict of interest.

Abbreviations

The following abbreviations are used in this manuscript:

CSEM	Controlled-source electromagnetic
TU Delft	Delft University of Technology
EM	Electromagnetic
ERT	Electrical resistivity tomography
MT	Magnetotelluric
SNR	Signal-to-noise ratio
FDEM	Frequency-domain electromagnetic
2D	Two-dimensional
1D	One-dimensional
3D	Three-dimensional

References

1. Pirouti, M.; Bagdanavicius, A.; Ekanayake, J.; Wu, J.; Jenkins, N. Energy consumption and economic analyses of a district heating network. *Energy* **2013**, *57*, 149–159. [CrossRef]
2. Mazhar, A.R.; Liu, S.; Shukla, A. A state of art review on the district heating systems. *Renew. Sustain. Energy Rev.* **2018**, *96*, 420–439. [CrossRef]
3. Directorate-General for Energy. Drivers of Recent Energy Consumption Trends Across Sectors in EU28. European Commission 2018. Available online: https://energy.ec.europa.eu/system/files/2018-09/energy_consumption_trends_workshop_report-september_2018_0.pdf (accessed on 17 May 2022).
4. Lake, A.; Rezaie, B.; Beyerlein, S. Review of district heating and cooling systems for a sustainable future. *Renew. Sustain. Energy Rev.* **2017**, *67*, 417–425. [CrossRef]
5. Chandrasekharam, D.; Bundschuh, J. *Low-Enthalpy Geothermal Resources for Power Generation*; CRC Press: Boca Raton, FL, USA, 2008. [CrossRef]
6. Muffler, P.; Cataldi, R. Methods for regional assessment of geothermal resources. *Geothermics* **1978**, *7*, 53–89. [CrossRef]
7. Barbier, E. Geothermal energy technology and current status: an overview. *Renew. Sustain. Energy Rev.* **2002**, *6*, 3–65. [CrossRef]
8. Munoz, G. Exploring for geothermal resources with electromagnetic methods. *Surv. Geophys.* **2014**, *35*, 101–122. [CrossRef]
9. Martín-Gamboa, M.; Iribarren, D.; Dufour, J. On the environmental suitability of high-and low-enthalpy geothermal systems. *Geothermics* **2015**, *53*, 27–37. [CrossRef]
10. Olasolo, P.; Juárez, M.; Morales, M.; Liarte, I.A. Enhanced geothermal systems (EGS): A review. *Renew. Sustain. Energy Rev.* **2016**, *56*, 133–144. [CrossRef]
11. Kaya, E.; Zarrouk, S.J.; O'Sullivan, M.J. Reinjection in geothermal fields: A review of worldwide experience. *Renew. Sustain. Energy Rev.* **2011**, *15*, 47–68. [CrossRef]
12. Bödvarsson, G.S.; Tsang, C.F. Injection and thermal breakthrough in fractured geothermal reservoirs. *J. Geophys. Res. Solid Earth* **1982**, *87*, 1031–1048. [CrossRef]
13. Stefansson, V.-đ. Geothermal reinjection experience. *Geothermics* **1997**, *26*, 99–139. [CrossRef]
14. Axelsson, G.; Stefánsson, V.; Xu, Y. Sustainable management of geothermal resources. In Proceedings of the International Geothermal Conference, Reykjavik, Iceland, 14–17 September 2003; pp. 40–48. Available online: https://orkustofnun.is/gogn/unu-gtp-sc/UNU-GTP-SC-22-11.pdf (accessed on 25 November 2022).

15. Axelsson, G.; Stefánsson, V.; Björnsson, G.; Liu, J. Sustainable management of geothermal resources and utilization for 100–300 years. In Proceedings of the World Geothermal Congress, Antalya, Turkey, 24–29 April 2005; Volume 8, pp. 40–48. Available online: https://www.geothermal-energy.org/pdf/IGAstandard/WGC/2005/0507.pdf (accessed on 24 November 2022).
16. Poulsen, S.; Balling, N.; Nielsen, S. A parametric study of the thermal recharge of low enthalpy geothermal reservoirs. *Geothermics* **2015**, *53*, 464–478. [CrossRef]
17. O'Sullivan, M.J.; Pruess, K.; Lippmann, M.J. State of the art of geothermal reservoir simulation. *Geothermics* **2001**, *30*, 395–429. [CrossRef]
18. Wang, Y.; Voskov, D.; Khait, M.; Saeid, S.; Bruhn, D. Influential factors on the development of a low-enthalpy geothermal reservoir: A sensitivity study of a realistic field. *Renew. Energy* **2021**, *179*, 641–651. [CrossRef]
19. Bruhn, D.F.; Wolf, K. Woning, M.; Nick, H.M.; Willems, C.J.L. The Delft Aardwarmte Project (DAP): providing renewable heat for the university campus and a research base for the geothermal community. In Proceedings of the World Geothermal Congress 2015, Melbourne, Australia, 19–25 April 2015. Available online: https://pangea.stanford.edu/ERE/db/WGC/papers/WGC/2015/35016.pdf (accessed on 3 August 2021).
20. Virieux, J.; Operto, S. An overview of full-waveform inversion in exploration geophysics. *Geophysics* **2009**, *74*, WCC1–WCC26. [CrossRef]
21. Nabighian, M.N. *Electromagnetic Methods in Applied Geophysics: Voume 1, Theory*; Society of Exploration Geophysicists: Houston, TX, USA, 1988. [CrossRef]
22. Nabighian, M.N. *Electromagnetic Methods in Applied Geophysics: Volume 2, Application, Parts A and B*; Society of Exploration Geophysicists: Houston, TX, USA, 1991. [CrossRef]
23. Schön, J.H. *Physical Properties of Rocks: Fundamentals and Principles of Petrophysics*; Elsevier: Amsterdam, The Netherlands, 2015. Available online: https://shop.elsevier.com/books/physical-properties-of-rocks/schon/978-0-08-100404-3 (accessed on 9 August 2021).
24. Balasco, M.; Lapenna, V.; Rizzo, E.; Telesca, L. Deep electrical resistivity tomography for geophysical investigations: The state of the art and future directions. *Geosciences* **2022**, *12*, 438. [CrossRef]
25. Chave, A.D.; Jones, A.G. *The Magnetotelluric Method: Theory and Practice*; Cambridge University Press: Cambridge, UK, 2012. [CrossRef]
26. Fraser Smith, A.; Coates, D. Large-amplitude ULF electromagnetic fields from BART. *Radio Sci.* **1978**, *13*, 661–668. [CrossRef]
27. Egbert, G.D. Robust multiple-station magnetotelluric data processing. *Geophys. J. Int.* **1997**, *130*, 475–496. [CrossRef]
28. Abdelfettah, Y.; Sailhac, P.; Larnier, H.; Matthey, P.; Schill, E. Continuous and time-lapse magnetotelluric monitoring of low volume injection at Rittershoffen geothermal project, northern Alsace–France. *Geothermics* **2018**, *71*, 1–11. [CrossRef]
29. Constable, S.; Srnka, L.J. An introduction to marine controlled-source electromagnetic methods for hydrocarbon exploration. *Geophysics* **2007**, *72*, WA3–WA12. [CrossRef]
30. Ziolkowski, A.; Slob, E. *Introduction to Controlled-source Electromagnetic Methods: Detecting Subsurface Fluids*; Cambridge University Press: Cambridge, UK, 2019. [CrossRef]
31. Myer, D.; Constable, S.; Key, K. Broad-band waveforms and robust processing for marine CSEM surveys. *Geophys. J. Int.* **2011**, *184*, 689–698. [CrossRef]
32. Colombo, D.; McNeice, G.W. Quantifying surface-to-reservoir electromagnetics for waterflood monitoring in a Saudi Arabian carbonate reservoir. *Geophysics* **2013**, *78*, E281–E297. [CrossRef]
33. Colombo, D.; McNeice, G.W. Surface to borehole CSEM | for waterflood monitoring in Saudi Arabia: Data analysis. In *SEG Technical Program Expanded Abstracts 2018*; Society of Exploration Geophysicists: Houston, TX, USA, 2018; pp. 868–872. [CrossRef]
34. Olufemi, O.; Bello, O.; Olaywiola, O.; Teodoriu, C.; Salehi, S.; Osundare, O. Geothermal Heat Recovery from Matured Oil and Gas Fields in Nigeria–Well Integrity Considerations and Profitable Outlook. In Proceedings of the 45th Workshop on Geothermal Reservoir Engineering, Stanford, CA, USA, 10–12 February 2020; pp. 1–12. Available online: https://pangea.stanford.edu/ERE/db/GeoConf/papers/SGW/2020/Bello.pdf (accessed on 18 May 2023).
35. DeVault, B.; Jeremiah, J. Tectonostratigraphy of the nieuwerkerk formation (delfland subgroup), west Netherlands basin. *AAPG Bull.* **2002**, *86*, 1679–1707. [CrossRef]
36. Donselaar, M.E.; Groenenberg, R.M.; Gilding, D.T. Reservoir geology and geothermal potential of the Delft Sandstone Member in the West Netherlands Basin. In Proceedings of the World Geothermal Congress, Melbourne, Australia, 19–25 April 2015; pp. 1–9. Available online: https://pangea.stanford.edu/ERE/db/WGC/papers/WGC/2015/12054.pdf (accessed on 18 May 2023).
37. Vardon, P.; Bruhn, D.; Steiginga, A.; Cox, B.; Abels, H.; Barnhoorn, A.; Drijkoningen, G.; Slob, E.; Wapenaar, K. A Geothermal Well Doublet for Research and Heat Supply of the TU Delft Campus. *arXiv* **2003**, arXiv:2003.11826. [CrossRef]
38. Keller, G.V.; Frischknecht, F.C. *Electrical Methods in Geophysical Prospecting*; Not available as an Electronic Version; Pergamon Press: Oxford, NY, USA, 1966; pp. 19–21.
39. Hunziker, J.; Thorbecke, J.; Slob, E. The electromagnetic response in a layered vertical transverse isotropic medium: A new look at an old problem. *Geophysics* **2015**, *80*, F1–F18. [CrossRef]
40. Werthmüller, D. An open-source full 3D electromagnetic modeler for 1D VTI media in Python: Empymod. *Geophysics* **2017**, *82*, WB9–WB19. [CrossRef]
41. Heagy, L.J.; Cockett, R.; Kang, S.; Rosenkjaer, G.K.; Oldenburg, D.W. A framework for simulation and inversion in electromagnetics. *Comput. Geosci.* **2017**, *107*, 1–19. [CrossRef]

42. Mittet, R.; Morten, J.P. Detection and imaging sensitivity of the marine CSEM method. *Geophysics* **2012**, *77*, E411–E425. [CrossRef]
43. Havsgård, G.B.; Jensen, H.R.; Kurrasch, A.; Jones, H.; Austin, P.; Thompson, A. *Low Noise Ag/AgCl Electric Field Sensor System for Marine CSEM and MT Applications*; Geoservices ASA: Lysaker, Norway, 2011. Available online: https://emgs.com/wp-content/uploads/2021/08/Low-Noise-Ag_AgCl-Electric-Field-Sensor-System-for-Marine-CSEM-and-MT-Applications.pdf (accessed on 6 January 2023).
44. Strack, K.-M. *Exploration with Deep Transient Electromagnetics*; Elsevier: Amsterdam, The Netherlands, 1992; Volume 373. Available online: https://www.researchgate.net/publication/288945453_Exploration_with_Deep_Transient_Electromagnetics (accessed on 27 June 2022).
45. Wirianto, M.; Mulder, W.; Slob, E. A feasibility study of land CSEM reservoir monitoring in a complex 3-D model. *Geophys. J. Int.* **2010**, *181*, 741–755. [CrossRef]
46. Jacobs, A.F.; Heusinkveld, B.G.; Holtslag, A.A. Long-term record and analysis of soil temperatures and soil heat fluxes in a grassland area, The Netherlands. *Agric. For. Meteorol.* **2011**, *151*, 774–780. [CrossRef]
47. Kaufman, A.A. The electrical field in a borehole with a casing. *Geophysics* **1990**, *55*, 29–38. [CrossRef]
48. Wu, X.; Habashy, T.M. Influence of steel casings on electromagnetic signals. *Geophysics* **1994**, *59*, 378–390. [CrossRef]
49. Swidinsky, A.; Edwards, R.N.; Jegen, M. The marine controlled source electromagnetic response of a steel borehole casing: Applications for the NEPTUNE Canada gas hydrate observatory. *Geophys. Prospect.* **2013**, *61*, 842–856. [CrossRef]
50. Orujov, G.; Streich, R.; Swidinsky, A. Modeling and inversion of electromagnetic data collected over steel casings: An analysis of two controlled field experiments in Colorado. *Lead. Edge* **2022**, *41*, 114–121. [CrossRef]
51. Heagy, L.J.; Oldenburg, D.W. Modeling electromagnetics on cylindrical meshes with applications to steel-cased wells. *Comput. Geosci.* **2019**, *125*, 115–130. [CrossRef]